

Received June 7, 2019, accepted July 1, 2019, date of publication July 9, 2019, date of current version July 26, 2019.

Digital Object Identifier 10.1109/ACCESS.2019.2927515

Biomechanical Analysis of the Lower Limb: A Full-Body Musculoskeletal Model for Muscle-Driven Simulation

MANUEL CARDONA^{1,2}, (Senior Member, IEEE), AND CECILIA E. GARCÍA CENA³

¹Centre for Automation and Robotic (CAR), Universidad Politécnica de Madrid (UPM), 28006 Madrid, Spain

²Robot and Intelligence Machines Research Group, Universidad Don Bosco (UDB), San Salvador 1116, El Salvador

³Centre for Automation and Robotic (CAR), Universidad Politécnica de Madrid (UPM), 28012 Madrid, Spain

Corresponding author: Manuel Cardona (manuel.cardona@udb.edu.sv)

The work of M. Cardona was supported in part by the Fundación Carolina, and in part by the Universidad Don Bosco during his research through the Doctoral Scholarship.

ABSTRACT Musculoskeletal model is a useful tool to evaluate the complex biomechanical problems, simulate and evaluate the injuries, estimate the muscle-tendon forces, and joint the torques during motion and predict the effects of orthopedic surgeries. Moreover, the musculoskeletal model is a rich source of information to develop robotics exoskeleton aiming to restore the normal gait after some injuries. This paper presents a full musculoskeletal model in an open-source framework to perform the biomechanical analysis of the human lower limb in order to simulate both healthy and pathological gait; 14 bones, 88 Hill-type muscle-tendon segments, ten ligament segments for each knee, and six joints for each lower limb were modeled. The model allows us to simulate different injuries of the lower limb, such as ictus, stroke, and so on, by sending different signal profiles to muscle-tendon segments, emulating the functional electrical stimulation (FES). At the same time, forces and torques could be computed for muscles and joints. Hence, the proposed model can be suitable not only to perform a complete biomechanical analysis for medical purposes but also for the exoskeleton controller design and actuators dimensioning. In order to validate the model, it was exported to Simulink environment to simulate the joints range of motion, muscle moment arm, and joint torque, and then, these data were compared with the medical literature. All simulations results show that the data from the model are according to the previously published works. Furthermore, the model was validated using the real data obtained by our own gait capture system and by CODA motion software for normal and pathological gait. Finally, the goodness-of-fit of our model was assessed using the root mean square error (RMSE) and the normalized mean square error (NMSE); the values of these indices suggest that the model estimated the kinematics and kinetics parameters of healthy and pathological gait successfully.

INDEX TERMS Exoskeleton, force, open source model, muscle-tendon, lower limb, rehabilitation robotics.

I. INTRODUCTION

Musculoskeletal models have been used successfully in many applications such as injuries analysis, surgeries evaluation and biomechanical analysis to determine forces and torques. Piazza and Delp [1] have used a model to predict the motions of knee implants during a step-up activity, Cazzola *et al.* [2], used a model to evaluate cervical spine injuries, Paul *et al.* [3] studied the effects of spinal cord injury on locomotor abilities, Arnold *et al.* [4], used a musculoskeletal model to estimate muscle-tendon length of the hamstrings and iliopsoas in patients with cerebral palsy to predict the biomechanical effect of a surgical intervention, Reinbolt *et al.* [5],

Rasmussen *et al.* [6], used a model to evaluate sport performance, Lee *et al.* [7], analyzed ankle muscles activities during gait, and Wang *et al.* [8], used a model to study the biomechanical characteristics of the gait.

In the literature, the reader can find several lower limb models, however, part of them are incomplete and/or based on an expensive software platform. For example, Delp *et al.* [9], created a model based on a dataset from 5 cadaver subjects, Klein Horsman [10] from a single cadaver limb, Arnold *et al.* [11] from 22 cadaver subjects, Carbone [12] from a single cadaver limb and Rajagopal *et al.* [13], have recently created a model from a dataset [14] obtained using MRI from 24 active, healthy subjects and a dataset [15] from 20 cadaver subjects, Lai *et al.* [16] have refined the musculoskeletal model presented by [13] in order to simulate

The associate editor coordinating the review of this manuscript and approving it for publication was Long Cheng.

pedalling and fast running. Moreover, all of these models are for biomechanical simulation exclusively and cannot be exported directly to a mechanical design tool.

The model presented in this paper is a full model of the lower limb, which could be linked to MATLAB® environment, then the biomechanical analysis can be easily extended to the mechanical synthesis stage of robotic mechanisms. Under this environment, it is possible to develop a control framework for the robotics exoskeleton combining biomechanical simulation, sensor information (EMG, EEG, inertial sensor, image data, etc) and muscle-driven simulations.

The aim of this paper is to present a complete model in an open source platform to facilitate the biomechanical analysis of the lower limb, integrate external sensory information, improve the design stage of rehabilitation exoskeletons and include biomechanical simulation into the control algorithm in order to build exoskeletons adapted to each patient and rehabilitation therapy. Furthermore, the model will allow to study differences in muscle synergies of a pathology and compare them with a normal gait which is crucial for the mechanical design of powered lower limb robotic exoskeleton.

In addition, all muscle-tendon activity can be estimated from this model. In clinical practice, these data are collected using invasive and/or non-invasive electromyography systems (EMG). Non-invasive EMG has a low sensitivity to discriminate between voluntary motor activity and deep muscle activity involved during limb movement, thus, invasive EMG would be needed. However, considering the ethical issues given by the International Ethical Guidelines for Biomedical Research Involving Human Subjects [17], it is not allowed to get these data in the context of some researches. Consequently, our model allows to estimate the muscle-tendon activity precisely.

This paper is organized as follows, first, the full musculoskeletal model of the lower limb is presented including the muscle-tendon architecture, ligaments of the knee, joint geometry, and the Simulink model. Next, the model is validated by comparing the obtained results (predicted from model) to previously published works (predicted from model and experimental results). Finally, the model is also validated with real data for a gait cycle for both normal and pathological subjects.

II. MUSCULOSKELETAL MODELING

A Musculoskeletal Model is composed of bones, muscle-tendon segments, ligaments and wrapping objects. The correct activation of each muscle group allows the motion of each joint. Among the software used for musculoskeletal modeling are SIMM, OpenSim, AnyBody and MSMS. SIMM and AnyBody are commercial software, OpenSim is free and open-source software and MSMS is a free software.

We selected MSMS because it runs under MATLAB/Simulink environment which is also suitable to design and validate control architectures for robotics exoskeletons.

TABLE 1. Musculoskeletal Modeling Software Comparison.

Software	Main Features
SIMM	-License: Commercial
	-Simulink Export: No native -Real-time viewing -Bone deformation modeling -Inverse kinematics utility
OpenSim	-License: Free
	-Simulink Export: No native -Muscle-driven forward dynamic (from data recorded) -Inverse kinematics utility -Allows dynamic simulations
AnyBody	-License: Commercial
	-Simulink Export: No native -Friction forces modeling -Inverse Dynamics utility -Allows simulations with implants
MSMS	-License: Free
	-Simulink Export: Native (directly) -Real-time data capture and viewing -Solidworks/OpenSim Importing tool Customization: -Muscle Fiber type -Maximum recruitment excitation value -Recruitment type -Apportion method

On the other hand, the interaction between OpenSim and Simulink is minimum, the researchers have to develop additional tools to communicate using the API provided. This interaction with Simulink enables us to evaluate different pathologies simply changing the signals introduced into the muscles.

In addition, MSMS can receive data in real time (a feature that does not have OpenSim) from signals coming from sensors such as an inertial measurement unit (IMU), the signals could be acquired and processed in any software like MATLAB or LabView and send them to MSMS to see the motion of the model. This is very important for data acquisition and visualization for real-time simulations in virtual reality environments with the subject in the loop, an application using this feature for an upper limb musculoskeletal modeling can be found in [18]. Another unique feature of MSMS is that allows not only to define the muscle fiber type but also to select the recruitment type, as well as to choose the apportion method and the maximum recruitment excitation value. The main disadvantage of MSMS is that there is no technical support or actualized documentation to use the software. Table 1, summarizes the main features of the most used biomechanical analysis software, whereas Table 2, summarizes the previously models reported.

A. THE MUSCULOSKELETAL MODEL

The proposed model in this paper was created based on the anatomical dataset reported by Arnold *et al.* [11] and Ward *et al.* [15]. Our model has been implemented using Musculoskeletal Modeling Software (MSMS). MSMS has

TABLE 2. Musculoskeletal Models Previously Reported. MTU:Muscle-Tendon Units. *MTU/Ligaments per leg.

Authors	Source	Main Drawbacks/Features	MTU/Ligaments*	Software	Year
Delp et al. [9]	5 cadavers	Musculotendon parameters are based on two studies of two and three cadavers	43/0	SIMM/OpenSim	1990
K. Horsman [10]	Single cadaver	Musculotendon parameters are based only in a Single cadaver, it is unclear how well this single subject represents other subjects	38/14	SIMM/OpenSim	2007
Arnold et al. [11]	21 cadavers	The model makes extensive use of ellipsoidal wrapping objects, this kind of objects does not have a closed-form solution for how a muscle path over them, which represents a high computational cost	44/0	SIMM/OpenSim	2010
Modenese et al. [19]	Single cadaver	Although the model was validated using EMG and hip contact forces (HCFs), it is unclear how well this single subject represents other subjects	38/14	SIMM/OpenSim	2011
R. Chauhan [20]	Arnold's Model	The model does not present any kind of validation. Also, the model does not appear to include wrapping objects, this means that is not possible to generate the right forces in muscles such as: Iliacus, Psoas or Gastrocnemius.	36/0	MSMS	2013
V. Carbone et al. [12]	Single cadaver	This model still reflects a single cadaver subject, and, thus, may be unsuitable for scaling to a wide range of subjects.	55/12	AnyBody	2015
Rajagopal et al. [13]	21 cadavers, 24 adults	It is not possible to obtain an equivalent model in Simulink. It is not possible to define: muscle fiber type , recruitment type, apportion method and the maximum recruitment excitation value. Also, can not be integrated with simulations of exoskeleton control systems.	40/0	OpenSim	2016
K.M. Lai [16]	Rajagopal's Model	It is not possible to obtain an equivalent model in Simulink. It is not possible to define: muscle fiber type , recruitment type, apportion method and the maximum recruitment excitation value. Also, can not be integrated with simulations of exoskeleton control systems.	40/0	OpenSim	2017
Our model	21 cadavers	As in all previous models, it does not include all the muscles of the lower limb. However, these muscles make little contribution to the moment generated by the joint, therefore, they do not significantly alter the results. However, the model can be exported directly to Simulink allowing us to use all the MATLAB toolboxes, also, is possible to generate functional electrical stimulation (FES) signals for muscle-driven simulations and receive data in real time from signals coming from sensors or third-party software.	44/10	MSMS	2019

the advantage that the model can be exported directly to Simulink allowing us to generate functional electrical stimulation (FES) signals for muscle-driven and send these signals to MSMS via UDP. Some previous successful works using MSMS have been reported for the upper limb [18], however, for the lower limb the reported models are incomplete [19] [20], without any kind of validation.

The musculoskeletal model of the lower limb includes both legs and consists of 14 body segments (torso, pelvis, left/right femur, left/right tibia, left/right patella, left/right

talus, left/right calcaneus and left/right toes), the inertial parameters for each body-segment were taken from Arnold *et al.* [11] and are shown in Table 3. It worth noting that biomechanical data used in our model are consistent with mean values for European adults and were taken from the medical literature.

The model is composed of 44 muscle-tendon actuators per leg, each actuator was modeled as a 3-element Hill-type muscle-tendon unit [21]–[23] as depicted in Fig. 1. For muscle-tendon with complex geometry (Adductor magnus,

TABLE 3. Mass (kg) and moments of inertia for the body segments (kg.m²). R: Right, L: Left.

Segment	Mass	I_{xx}	I_{yy}	I_{zz}
Torso	26.8266	1.4745	0.7555	1.4314
Pelvis	11.777	0.1028	0.0871	0.0579
Femur R/L	9.3014	0.1339	0.0351	0.1412
Tibia R/L	3.7075	0.0504	0.0051	0.0511
Patella R/L	0.0862	2.87E-6	1.311E-5	1.311E-5
Talus R/L	0.1	0.001	0.001	0.001
Calcaneus R/L	1.25	0.0014	0.0039	0.0041
Toe R/L	0.2166	1E-4	2E-4	0.001

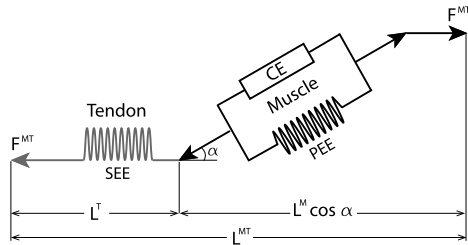


FIGURE 1. Hill-type muscle-tendon model. CE: Contractile element, PEE: Parallel elastic element, SEE: Serial elastic element, α : Pennation angle.

gastrocnemius, gluteus maximus, gluteus medius, gluteus minimus) the whole muscle was divided into multiple segments and the constraint of the muscle-tendon path was modeled by moving points and wrapping objects.

Each muscle is described by an active contractile element (CE) that generates the active force and a passive parallel-elastic element (PEE) that includes a small viscosity for stability purposes. The model is completed with a non-linear series-elastic element (SEE) representing the mechanical properties of the tendon.

The instantaneous length of a muscle-tendon unit (L^{MT}) is given by the tendon length (L^T), the muscle length (L^M) and the pennation angle of the muscle (α), thus:

$$L^{MT} = L^T + L^M \cos \alpha \quad (1)$$

For a muscle, the force-velocity relationship of the CE is given by a non-linear first order model (Fig. 2c) and the force-length property is defined by a non-linear Gaussian curve (Fig. 2b). The force in PEE is a function of its length and is related according to an exponential curve (Fig. 2b).

The stress-strain curve for a tendon is considered linear (Fig.2a) and whose normalized force is a function of the tendon strain (ϵ) which is calculated from the tendon slack length (L_s^T), we have considered when the muscle develop maximum isometric force (F_0^M) the tendon strain is 3.3 %.

Both, the muscle force (F^M) and tendon force (F^T) are normalized by maximum isometric muscle force F_0^M , while, tendon length (L^T) and muscle-fiber length (L^M) are normalized by optimal muscle-fiber length (L_0^M).

The muscle force is the sum of an active force generates by the CE and a passive force generates by the PEE, that is:

$$F^M = [F_{act}(CE) + F_{pass}(PEE)] \quad (2)$$

The passive force exists only at lengths greater than their optimal muscle-fiber length, the force is passive since it exists whether or not the muscle is active, and it is a function of the normalized fiber-length. The active force developed by the muscle depends on factors such as normalized fiber length, speed of contraction and muscle activation. Therefore, using the curves depicted in Fig. 2, the muscle force (normalized by peak isometric muscle force, F_0^{MN}) can be computed from:

$$F^M = aF^L(L^N)F^V(V^N) + F^{PE}(L^N) \quad (3)$$

where, a is the activation level of the muscle ($a_{min} \leq a \leq 1$), F^L the active force-length curve as a function of the normalized muscle length (L^N), F^V the force-velocity curve as a function of the normalized velocity (V^N) and F^{PE} is the passive force-length curve as a function of the normalized muscle length (L^N). Muscle-tendon force is determined by a given activation level and muscle-tendon length.

B. MUSCLE-TENDON ARCHITECTURE

The Hill-type muscle model presented in the previous section defines the muscle force generation, MSMS Software implements this model and requires the following morphometrics parameters: optimal fascicle length, optimal tendon length, maximum muscle-tendon length, and muscle mass.

The complete model is depicted in Fig. 3 and the morphometry is described in Table 4. The muscle-tendon parameters were based from those reported by Arnold *et al.* [11], Ward *et al.* [15], and Rajagopal *et al.* [13], and are the most recent dataset available. The cadavers (21 subjects) from which muscle-tendon architecture parameters were measured [15], had an average weight of 82.7 ± 15.2 kg and height of 168.4 ± 9.3 cm.

C. LIGAMENTS OF THE KNEE

The function of a ligament is to restrict the joint motion and stabilize the joint [24], the ligaments are composed mainly of collagen fibers which are not highly elastic and present failure at low elongations or strain. Under normal conditions, the maximum strain rate is 5% or less and the failure of each individual fiber begins at 8% of strain, the stress-strain relationship is shown in Fig. 4.

The ligament tension is a function of its length, for low strains, the function is assumed to be non-linear and become linear for strains higher that certain level [25], [26], the mechanical properties can be described by a force-length curve modeled by:

$$f = \begin{cases} 0 & e < 0 \\ \frac{1}{4}ke^2/e_l & 0 \leq e \leq 2e_l \\ k(e - e_l) & e > 2e_l \end{cases} \quad (4)$$

where, f is the tensile force, k is the ligament stiffness, e_l is the transition strain that was considered 0.03 [25], [27],

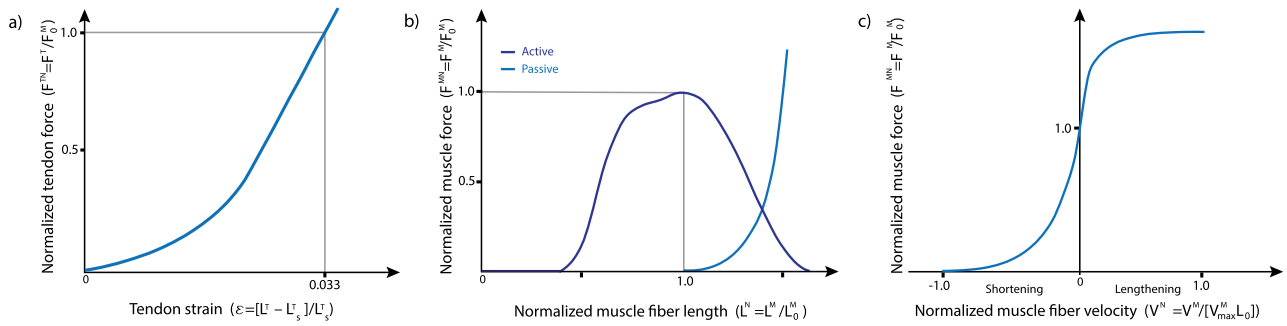


FIGURE 2. Hill-type muscle model curves to estimate tendon and muscle forces. a) Tendon force-length curve, tendon force (F^T) is normalized to maximum isometric force (F_0^M) and tendon length (L^T) is normalized to tendon slack length (L_s^T), the normalized tendon force (F^{TN}) is a function of the tendon strain (ϵ), b) Active and passive muscle force-length curve, muscle force (F^M) is normalized to maximum isometric force (F_0^M) and muscle fiber length (L^M) is normalized to optimal fiber length (L_0^M), the active isometric fiber force is a function of a muscle activation level (α) and fiber length (L^M), the passive fiber force is a function of the normalized muscle fiber length (L^{MN}), c) Muscle force-velocity curve, muscle active force (F^M) is normalized to maximum isometric force (F_0^M) and velocity (V^M) is normalized to the maximum muscle contraction velocity (V_{max}^M). Negative normalized velocities values correspond to concentric contractions.

TABLE 4. Morphometrics values of the model, based and adapted from Arnold *et al.* [11], Ward *et al.* [15], and Rajagopal *et al.* [13].

Muscle Segment	Optimal Fascicle Length (cm)	Optimal Tendon length (cm)	Max. MT Length (cm)	Mass (g)	PCSA (cm ²)	Max. Force (N)
Adductor brevis	10.30	3.60	16.68	104.3715	9.55958	303.994
Adductor longus	10.82	13.00	28.58	144.0863	12.5628	399.499
Adductor magnus distal	17.72	9.00	32.06	191.49	10.1949	324.2
Adductor magnus ischial	15.62	22.1	45.26	168.8	10.1949	324.2
Adductor magnus middle	13.77	4.8	22.8	148.8078	10.1949	324.2
Adductor magnus proximal	10.56	4.3	17.83	114.1184	10.1949	324.2
Biceps femoris long head	9.76	32.2	50.35	229.425	22.1761	705.2
Biceps femoris short head	11.03	10.4	25.72	116.1091	9.9308	315.8
Extensor digitorum longus	6.93	36.73	52.39	79.7874	10.8616	345.4
Extensor hallucis longus	7.48	33.15	48.76	41.14	5.1886	165
Flexor digitorum longus	4.46	37.77	50.68	40.794	8.6289	2274.4
Flexor hallucis longus	5.27	35.6	49.04	76.7312	13.7358	436.8
Gastrocnemius lateral head	5.88	38.2	52.90	118.854	19.069	606.4
Gastrocnemius medial head	5.1	40.08	54.22	222.359	41.132	1308
Gemelli	2.4	3.9	7.56	8.72	3.4276	109
Gluteus maximus superior	14.73	5.0	23.68	268.135	17.1729	546.1
Gluteus maximus middle	15.69	7.33	27.62	408.2015	24.544	780.5
Gluteus maximus inferior	16.65	7.02	28.40	291.9855	16.544	526.1
Gluteus medius anterior	7.33	5.65	15.58	215.2821	27.707	881.099
Gluteus medius middle	7.33	6.6	16.72	150.6315	19.3867	616.5
Gluteus medius posterior	7.33	4.6	14.32	171.522	22.075	702
Gluteus minimus anterior	6.8	1.6	10.08	40.8	5.6603	180
Gluteus minimus middle	5.6	2.6	9.84	35.466	5.9748	190
Gluteus minimus posterior	3.8	5.1	10.68	27.23	6.761	215
Gracilis	22.78	16.6	47.26	104.256	4.3176	137.3
Iliacus	10.66	9.4	24.07	220.98	19.556	621.9
Patellar tendon	5.0	0.5	6.6	0.1666	0.03144	1.0
Pectineus	13.3	0.1	16.08	78.47	5.566	177
Peroneus brevis	4.54	14.81	23.22	46.2928	9.619	305.9
Peroneus longus	5.08	33.3	46.06	110.6254	20.544	653.299
Peroneus tertius	7.9	10.0	21.48	23.7	2.83	90
Piriformis	2.6	11.5	16.92	25.6533	9.308	296
Psoas	11.69	9.7	25.67	186.923	15.0849	479.7
Quadratus femoris	5.4	2.4	9.36	45.72	7.9874	253.99
Rectus femoris	7.59	34.6	50.63	214.746	26.691	848.8
Sartorius	40.3	11.0	61.56	152.468	3.569	113.5
Semimembranosus	6.9	34.8	50.04	267.421	36.562	1162.7
Semitendinosus	19.3	24.5	52.56	194.2	9.4937	301.9
Soleus	4.4	28.15	39.06	525.93	112.76	3585.899
Tensor fascia latae	9.5	45	65.4	49.083	4.874	155
Tibialis anterior	6.83	24.1	37.12	153.379	21.1855	673.7
Tibialis posterior	3.78	28.18	38.35	114.1055	28.4779	905.599
Vastus intermedius	9.93	10.6	24.64	339.0102	32.2075	1024.2
Vastus lateralis	9.94	13.0	27.53	747.289	70.9245	2255.4
Vastus medialis	9.68	11.2	25.06	465.833	45.399	1443.7

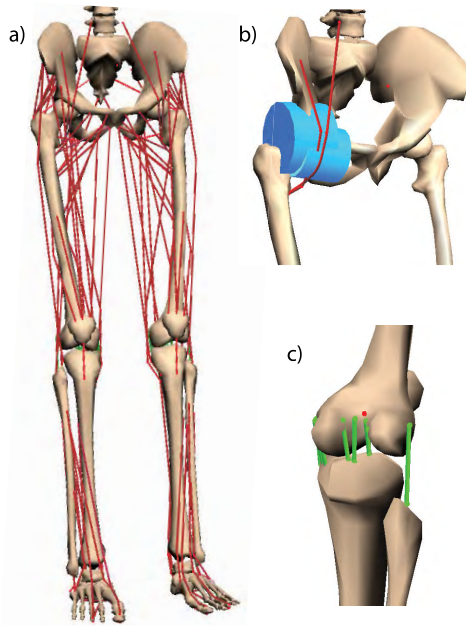


FIGURE 3. Musculoskeletal model of the lower limb. a) Full model with the 44 Hill-type muscle tendon units, b) Example of 2 wrapping objects to constrain the muscle-tendon path, c) Ligaments of the right knee.

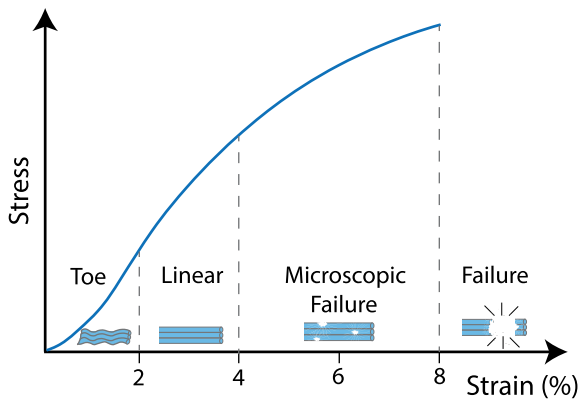


FIGURE 4. Stress-strain curve for a ligament. For less than 2% of strain we have the toe region, between 2% and 4% the ligament returns to its original length when is unloaded, between 4% and 8% microscopic failures can appear and after 8% a macroscopic failure (rupture) is presented.

e is the strain and can be determined from $e = (l - l_0)/l_0$, where l is the ligament length and l_0 is the zero-load length.

In the reference joint position (reference posture), we have the reference length of the ligament (l_r), and the strain rate corresponding is called the reference strain (e_r), this two parameters determine the zero-load length (l_0), thus,

$$l_0 = \frac{l_r}{e_r + 1} \tag{5}$$

The model presented includes 10 ligament segments per leg, the anterior and posterior cruciate ligaments (ACL, PCL) were represented by an anterior and posterior bundle (aACL, aPCL, pACL, pPCL). The lateral collateral ligament (LCL)

TABLE 5. Parameters for each ligament bundle. † Force at 5% stretch. Stiffness values were taken from [28].

Bundle	Stiffness (N)	l_r (cm)	e_r (%)	† Force (N)
aACL	1500	3.22	0.02	31.25
pACL	1600	2.57	-0.04	33.33
aPCL	2600	3.26	-0.13	54.17
pPCL	1900	2.91	-0.14	39.58
LCL	2000	5.65	0.01	41.67
aMCL	2500	6.98	-0.05	52.08
iMCL	3000	7.32	0.02	62.50
pMCL	2500	8.73	0.01	52.08
aDMCL	2000	3.63	-0.08	41.67
pDMCL	4500	3.57	-0.01	93.75

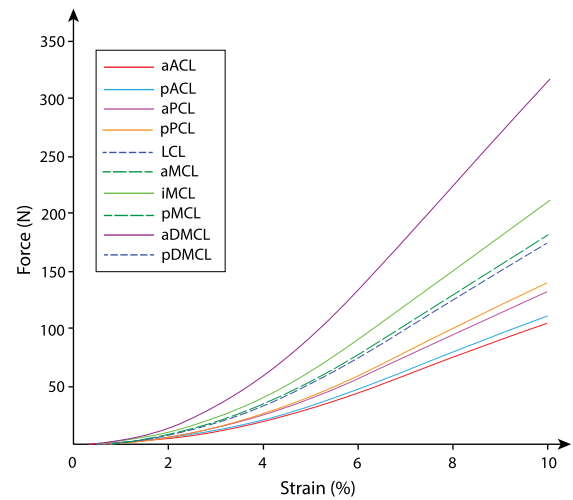


FIGURE 5. Strain-Force Curve for the ligament bundles.

was represented by a single bundle. The medial collateral ligament (MCL) was represented by 5 bundles, 3 bundles representing the superficial fibers: anterior, posterior and intermediate bundles (aMCL, pMCL, iMCL) and 2 deep bundles: anterior deep bundle and posterior deep bundle (aDMCL, pDMCL). The reference parameters for each ligament bundle is shown in Table 5 and the force-length curves are depicted in Fig. 5.

D. JOINT GEOMETRY

The model has 6 joints (hip, knee, ankle, subtalar, metatarsophalangeal, patellofemoral) allowing 7 active and 3 passive degrees of freedom (DoF) per leg.

The hip joint was modeled as a spherical joint allowing 3 DoF. The knee, ankle, metatarsophalangeal and subtalar were modeled as revolute joints, allowing one degree of freedom per joint.

The joint axes are depicted in Fig. 6, the range of motion (ROM) were taken from Kapandji [29], Moromizato *et al.* [30], and Arnold *et al.* [11] and are presented in Table 6.

The patellofemoral joint was modeled as a planar motion allowing 3 passive DoF: translation along x -axis (axis s_9 , Fig. 6), translation along y -axis (axis s_{10} , Fig. 6), rotation about z -axis (axis s_8 , Fig. 6). These translations and rotations

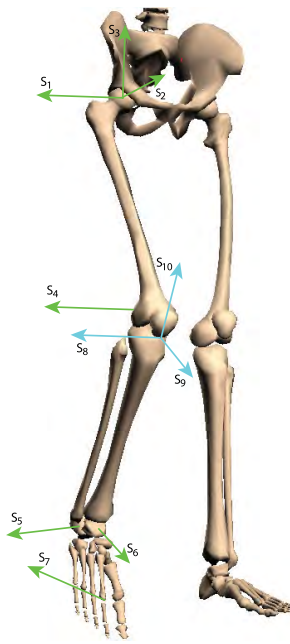


FIGURE 6. Joints Rotation and Translation Axes.

TABLE 6. Joints and range of motion (ROM). MTP:Metatarsophalangeal.

Joint	Action	ROM
Hip	Extension/Flexion	$-30^\circ/120^\circ$
	Abduction/Adduction	$-50^\circ/30^\circ$
	External/Internal Rotation	$-40^\circ/40^\circ$
Knee	Flexion/Extension	$-120^\circ/0^\circ$
Ankle	Plantar/Dorsal Flexion	$-40^\circ/30^\circ$
Subtalar	Eversion/Inversion	$-30^\circ/30^\circ$
MTP	Extension/Flexion	$-20^\circ/20^\circ$

are function of the knee flexion angle and can be described using splines as shown in Fig 7a, 7b and 7c respectively.

Thus, using interpolation for Fig. 7, the patellofemoral kinematics can be found using the following polynomials:

$$T_x = -9.657\theta^3 - 29.21\theta^2 + 17.08\theta + 0.157 \quad (6)$$

$$T_y = -3.497\theta^4 - 13.17\theta^3 + 9.276\theta^2 + 48.78\theta - 0.0281 \quad (7)$$

$$R_z = -0.1275\theta^5 - 0.8068\theta^4 - 1.945\theta^3 - 2.24\theta^2 - 0.2674\theta + 0.001728 \quad (8)$$

where T_x and T_y is the translation (mm) about x -axis and y -axis respectively, R_z is the rotation (radians) about z -axis, and θ is the knee angle in radians.

Due the patella has a passive movement, its location (position and orientation) is modeled as a function of the knee angle, however, MSMS does not allow to implement it. To overcome this problem a subsystem was created in Simulink and the motion was modeled as a function of the knee angle using (6), (7) and (8).

E. SIMULINK MODEL

One of the unique features of MSMS is the ability to export the model directly to Simulink. This represents a huge advantage because it allows: Set activation signals (muscle-driven simulation); measure angles, speeds, accelerations, torques and forces in the joints; integrate sensors as well as apply control strategies and integrate all the well-know MATLAB's toolboxes.

The Simulink model is composed by a drivers block with the muscle-tendons features (morphometry, fiber type and muscle path) in which the muscle-signals are set, a block representing the bone segments (SimMechanics block), an UDP block to send the signals to MSMS and a block that generates a file (".msm") used by MSMS as a source animation file. Fig. 8 shows the Simulink equivalent block diagram and its relation with MSMS.

III. TESTING AND VALIDATION

In order to validate the model presented, several tests were performed, the muscle-tendon segments were activated simulating the functional electrical stimulation (FES). Then, the results obtained were compared with both results presented in the literature and experimental data.

A. VALIDATION BY COMPARING WITH PREVIOUSLY PUBLISHED WORKS

Once the model is exported to Simulink, we can activate the necessary muscle-tendons groups to perform the movements required.

Given this set of activation signals which represents the functional electrical stimulation (FES) and ranges from 0 (minimum activation level) to 1 (maximum activation level), the model allows us to estimate:

- Joint position, velocity, and acceleration
- Joint forces and torques
- Muscle and ligaments lengths
- Muscle and joint moment arms

The activation signal for each muscle-tendon unit is a 0 to 1 pulse train with a pulse-width of 50% [31]. An active delay between each signal is set in order to shift agonist-antagonist muscles interactions.

The amplitude of the signals corresponds with the percentage of muscle activation (0% to 100%). That is, 100% for a healthy subject.

To test the model the hip flexion/extension, hip abduction/adduction, and knee flexion/extension was simulated, the muscle-tendon group activated is shown in Table 7.

The validation of the model was tested by comparing the obtained results (model predicted) to previously published works. Fig. 9 to 12 shows knee flexion moment arms (obtained directly from MSMS) of muscles crossing the knee and compare the results predicted by Arnold *et al.* [11] model, and those obtained from experimental measurements by Buford *et al.* [32] and Spoor and van Leeuwen [33] with our model.

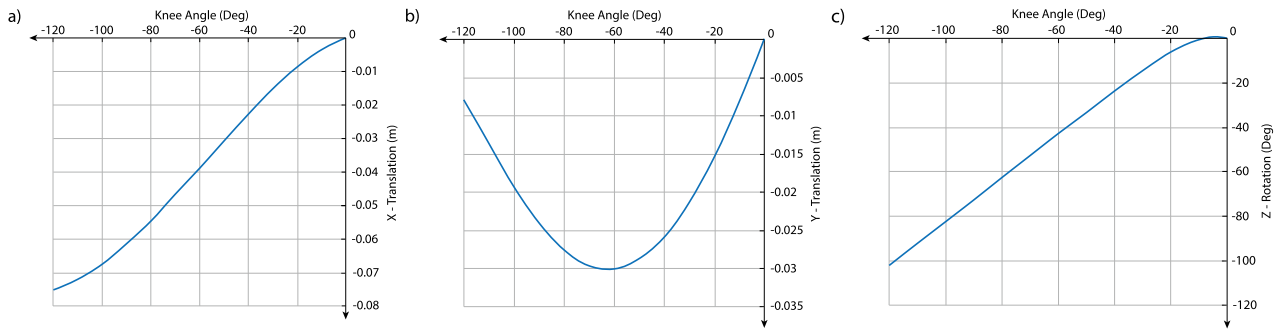


FIGURE 7. Patellofemoral joint position and orientation parameterized by the knee flexion angle. a) Patella translation along x-axis as a function of the knee angle, b) Patella translation along y-axis as a function of the knee angle, c) Patella rotation about z-axis as a function of the knee angle.

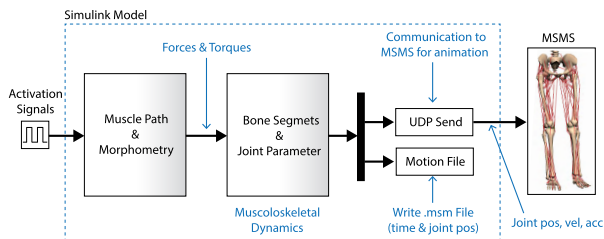


FIGURE 8. Simulink block model & MSMS integration.

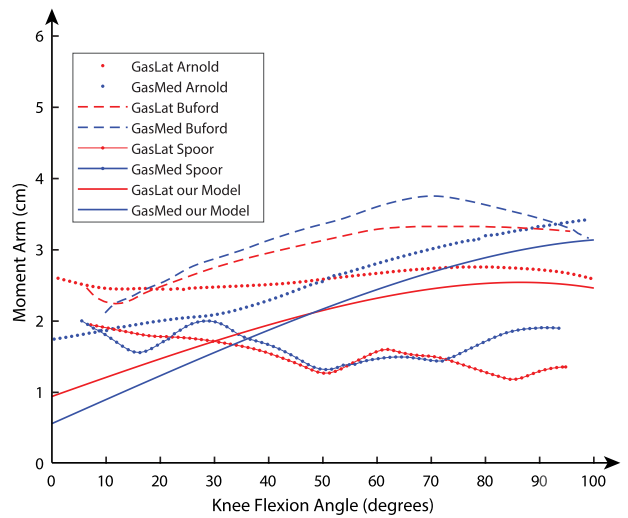


FIGURE 9. Moment arms of biceps femoris short head (BFSH) and biceps femoris long head (BFLH) muscles during knee flexion.

According to the results, the values obtained are within the bounds of this previously reported works. For instance, the maximum knee flexion moment arm predicted by our model for the biceps femoris short head was 3.35 cm at 70° of knee flexion angle, the values reported by Arnold *et al.* [11] predict that the peak value is 3.3 cm at 70°. In the case of the biceps femoris long head, the maximum knee flexion moment arm predicted by our model was 3.31 cm at 54° of flexion angle and the values reported by Arnold *et al.* [11] suggest a maximum knee flexion moment arm of 3.0 cm at 55°.

FIGURE 10. Moment arms of gastrocnemius lateral head (GasLat) and gastrocnemius medial head (GasMed) muscles during knee flexion.

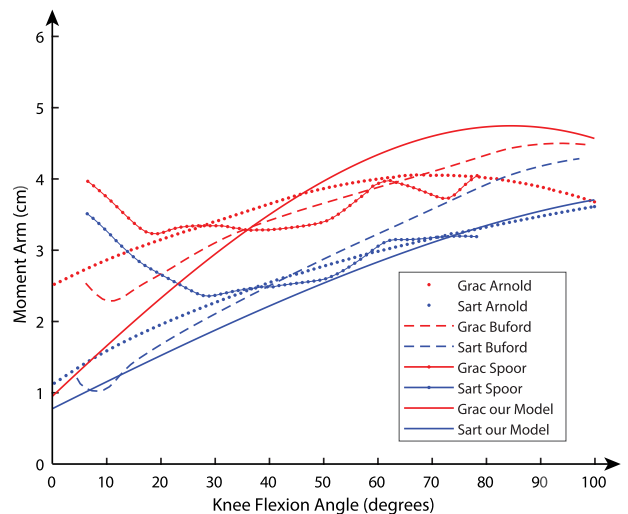










FIGURE 11. Moment arms of gracilis (Grac) and sartorius (Sart) muscles during knee flexion.

Maximum isometric joint moments for knee flexion/extension predicted by our model (Fig. 13) were compared to results reported in a previous model described by

TABLE 7. Lower limb joint movements and their agonist muscle-tendon groups.

Action	Muscle-Tendon	Movement
Hip Flexion	Adductor brevis	
	Adductor longus	
	Gluteus medius anterior	
	Gracilis	
	Iliacus	
	Pectineus	
	Psoas	
	Rectus femoris	
Hip Extension	Sartorius	
	Tensor fascia latae	
	Biceps femoris short head	
	Gluteus maximus superior	
	Gluteus maximus middle	
	Gluteus maximus inferior	
	Gluteus medius middle	
	Gluteus medius posterior	
Hip Abduction	Semimembranosus	
	Semitendinosus	
	Gluteus medius anterior	
	Gluteus medius middle	
	Gluteus medius posterior	
	Gluteus minimus anterior	
Hip Adduction	Gluteus minimus middle	
	Gluteus minimus posterior	
	Adductor Brevis	
	Adductor longus	
	Adductor magnus distal	
Knee Flexion	Adductor magnus ischial	
	Adductor magnus middle	
	Biceps femoris long head	
	Biceps femoris short head	
	Gastrocnemius lateral head	
	Gastrocnemius medial head	
	Gracilis	
	Sartorius	
Knee Extension	Semimembranosus	
	Semitendinosus	
	Patellar tendon	
	Rectus femoris	
	Vastus intermedius	
Ankle Dorsiflexion	Vastus lateralis	
	Vastus medialis	
	Extensor digitorum longus	
	Extensor hallucis longus	
Ankle Plantarflexion	Peroneus tertius	
	Tibialis anterior	
	Flexor digitorum longus	
	Extensor hallucis longus	
	Gastrocnemius lateral head	
	Gastrocnemius medial head	
	Peroneus brevis	
	Peroneus longus	
Soleus		

Arnold *et al.* [11] and Delp *et al.* [9], and experimental data reported by Anderson *et al.* [34]. The values were obtained with a hip flexion angle of 70° and an ankle angle of 0°

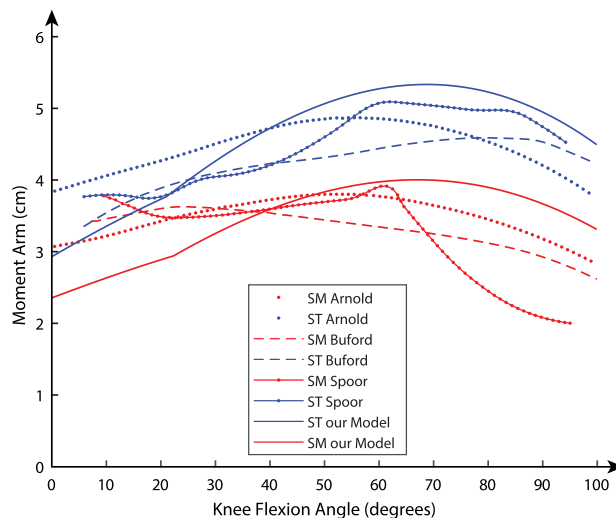


FIGURE 12. Moment arms of semimembranosus (SM) and semitendinosus (SM) muscles during knee flexion.

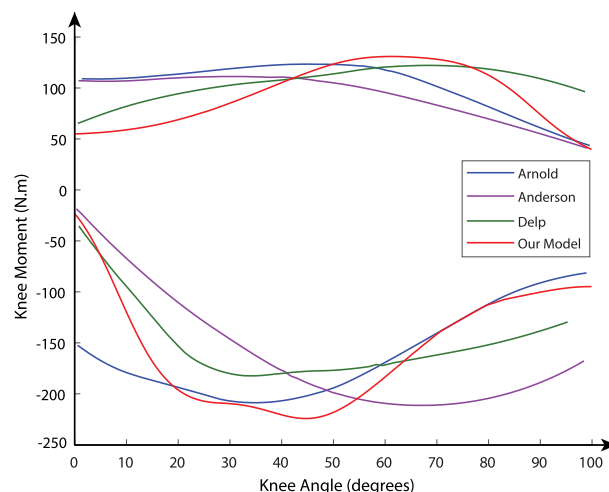


FIGURE 13. Maximum isometric knee moments. Positive values of the moment (upper curves) correspond with knee flexion and negative values with knee extension (lower curves).

to match with those used in previous works. As depicted in Fig. 13 the values predicted by our model were very similar, for instance, the model predicted a maximum knee flexion moment of 130 N.m at 58°, while Arnold *et al.* [11] reported a knee flexion peak of 122 N.m at 48°.

Maximum isometric joint moments for ankle dorsiflexion and plantarflexion predicted by our model (Fig. 14) were compared to results predicted by Arnold *et al.* [11] and Delp *et al.* [9] models, and experimental data reported by Anderson *et al.* [34]. The values were obtained with a knee flexion angle of 80° to match with those used in the previous works. As depicted in Fig. 14 the values predicted by our model were also very similar, for instance, the model predicted a maximum ankle dorsiflexion moment of 43 N.m at -6.1°, while Arnold *et al.* [11] reported an ankle dorsiflexion peak of 47 N.m at -7°.

The Simulink model was validated sending activation signals (simulating FES) to the corresponding muscles for

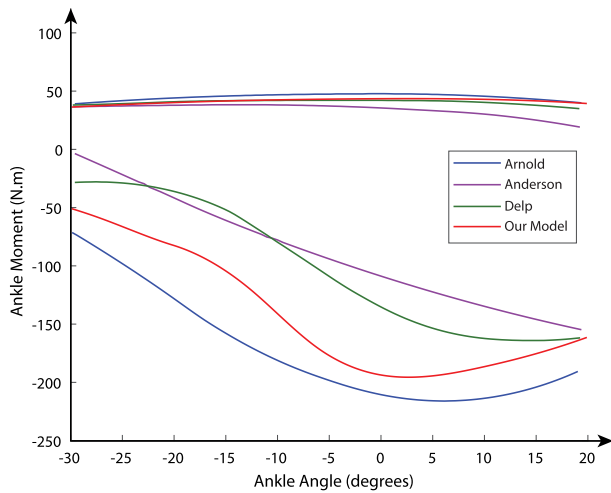


FIGURE 14. Maximum isometric ankle moments. Positive values of the moment (upper curves) correspond with ankle dorsiflexion and negative values with ankle plantarflexion (lower curves).

hip flexion (Table 6) and comparing the results with previously reported works. Fig. 15 depict parts of the Simulink model. Fig. 16 shows the results obtained by our model and the models described by Arnold *et al.* [11], Rajagopal *et al.* [13] and Lai *et al.* [16], and experimental data reported by Anderson *et al.* [34] and Riener and Edrich [35].

According to Fig. 16, the values predicted by our Simulink model were very similar for those obtained previously, for both reported models and values obtained experimentally. Table 8 summarizes the moment arms whereas Table 9 summarizes the maximum isometric moments obtained by our model and previously reported works (from early models and experimental results).

It is worth mentioning that many models are based on datasets previously reported, as in our case, however, none of the models generate identical results, this is due to the fact that, although the same morphometric values of the muscle-tendon have been used, the origin and insertion points of the muscle-tendon units, as well as the location, fiber type settings (recruitment type, apportion method, maximum recruitment excitation value), type and number of wrapping objects are not the same.

B. VALIDATION BY COMPARING WITH REAL DATA

The model was also tested over a gait cycle for both normal and pathological gait. For normal gait, the functional electrical stimulation (FES) signals applied to the muscles of the model (Simulink) over the gait cycle were selected according to medical literature (see appendix A). Thus, the results were compared with the previously published work reported by Miroslav *et al.* [40]. Moreover, the normal gait was also registered by our own wireless gait capture system (Fig. 17) that consist of three wireless 9-axis inertial measurement unit (IMU) modules, each module consists of a high-precision 3-axis gyroscope, 3-axis accelerometer, 3-axis geomagnetic sensor, and a 32 bits high-performance MCU,

TABLE 8. Moment arms summary. Arnold *et al.* [11] values were obtained from early model while Spoor and van Leeuwen [33] and Buford *et al.* [32] from experimental results. NR: Not reported, BFSH: Bicep femoris short head, BFLH: Biceps femoris long head, GasLat: Gastrocnemius lateral head, GasMed: Gastrocnemius medial head.

Muscle	Author	Moment Arm (cm)	Angle (deg)
BFSH	Arnold	3.3	70
	Spoor	NR	NR
	Buford	2.4	65
	Our Model	3.35	70
BFLH	Arnold	3	55
	Spoor	2.1	60
	Buford	3	55
	Our Model	3.31	54
GasLat	Arnold	2.8	80
	Spoor	1.7	62
	Buford	3.3	70
	Our Model	2.6	86
GasMed	Arnold	3.45	100
	Spoor	2	29
	Buford	3.75	70
	Our Model	3.2	99
Gracilis	Arnold	4.1	70
	Spoor	4.4	85
	Buford	4.5	92
	Our Model	4.7	86
Sartorius	Arnold	3.7	100
	Spoor	3.4	72
	Buford	4.3	94
	Our Model	3.8	102
Semimembranosus	Arnold	3.85	50
	Spoor	3.9	62
	Buford	3.7	25
	Our Model	4	66
Semitendinosus	Arnold	4.9	55
	Spoor	5.1	62
	Buford	4.6	82
	Our Model	5.3	68

allowing us to solve the current real-time motion posture quickly with a high accuracy (0.05°). Furthermore, the normal gait was registered using the Cartesian Optoelectronic Dynamic Anthropometer (CODA®) professional software at Physiotherapy School ONCE in Madrid. The results for the hip flexion/extension (HFE), knee flexion/extension (KFE), and ankle flexion/extension (AFE) are shown in Fig. 18.

The gray area corresponds to values obtained by CODA® software for fifteen healthy subjects. The root mean square error (RMSE) and the normalized mean square error (NMSE) for hip flexion/extension obtained by our model was 2.222 degrees and 2.743 % respectively, for knee flexion/extension the RMSE and NMSE was 2.793 degrees and 0.752 %, and for ankle flexion/extension the RMSE and NMSE was 0.9619 degrees and 1.7361 % respectively.

For pathological gait, the muscle level activation profile for each muscle-tendon unit used in our model was selected according to the literature and those muscle-tendon activation reported by Lencioni *et al.* [41], and correspond to persons with Multiple Sclerosis (PwMS). Furthermore, the gait cycle

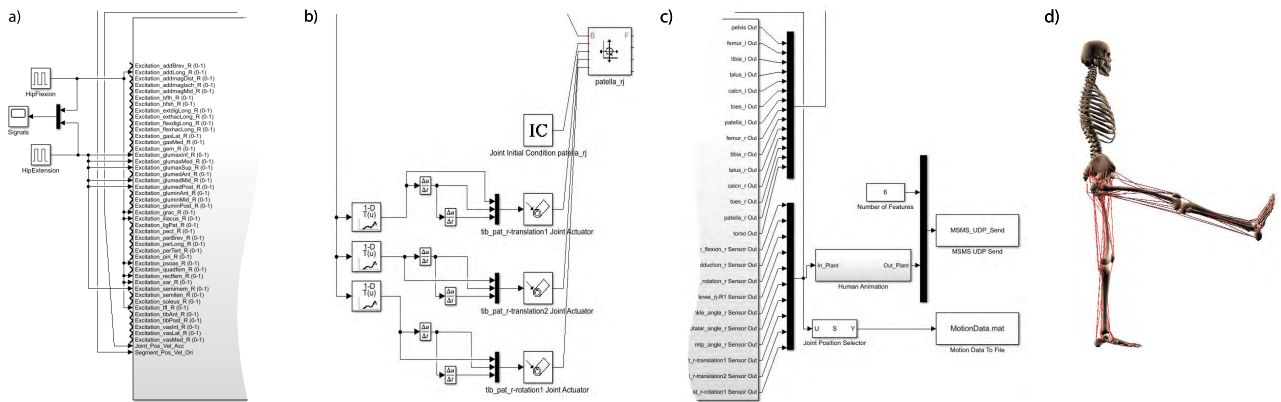


FIGURE 15. Simulink model. Simulation time 1 second, maximum hip flexion 73°. a) Activation signals for Hip Flexion, b) Patella splines implementation for patella location as a function of the knee angle c) Simulink UDP blocks communication and motion file (.msm) generator d) Model final position in MSMS after simulation, data received from Simulink.

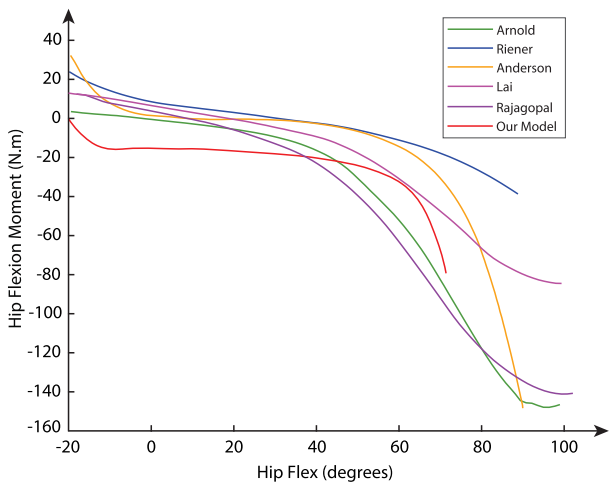


FIGURE 16. Passive hip flexion moment. The values were obtained using the Simulink model.

TABLE 9. Maximum isometric joint moments summary. Arnold et al. [11] and Delp et al. [9] values were obtained from early models while Anderson et al. [34], Murray et al. [36], Van Eijden et al. [37], Marsh et al. [38] and Sale et al. [39] from experimental results.

Movement	Author	Moment (N.m)	Angle (deg)
Knee Flexion	Our Model	130	58
	Arnold	122	48
	Anderson	112	28
	Murray	91	30
	Delp	123	66
Knee Extension	Our Model	224	45
	Arnold	210	36
	Anderson	212	68
	Van Eijden	240	60
Ankle Dorsiflexion	Our Model	43	-6.1
	Arnold	47	-7
	Anderson	38	-16
	Marsh	48	-10
Ankle Plantarflexion	Our Model	194	3
	Arnold	215	7
	Anderson	156	20
	Sale	170	15
Delp	165	15	

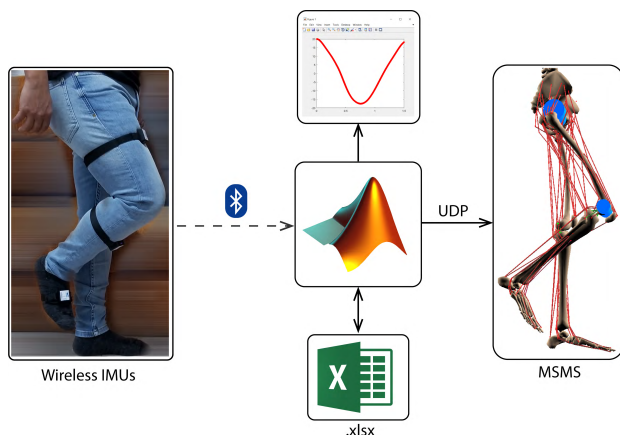


FIGURE 17. Wireless gait caption system.

for a PwMS was obtained using CODA[®] software at Physiotherapy School ONCE in Madrid, The results for the hip flexion/extension are shown in Fig. 19.

The gray area corresponds to values obtained by CODA[®] software for fifteen PwMS. The RMSE and NMSE obtained by our model respect to a particular PwMS case of study (obtained from CODA[®] software, light blue plot) were 2.542 degrees and 3.650 % respectively, for knee flexion/extension the RMSE and NMSE was 3.685 degrees and 1.733 %, and for ankle flexion/extension the RMSE and NMSE was 1.828 degrees and 0.5765 % respectively. Table 10 summarize the errors obtained by our model for both estimation, normal and pathological gait.

Furthermore, the absolute errors obtained by our estimation respect to IMU data for normal subjects and respect to CODA[®] data for pathological subjects are shown in Fig. 20.

According to the results for the gait cycle analysis, we can observe that the curves obtained by our model follow,

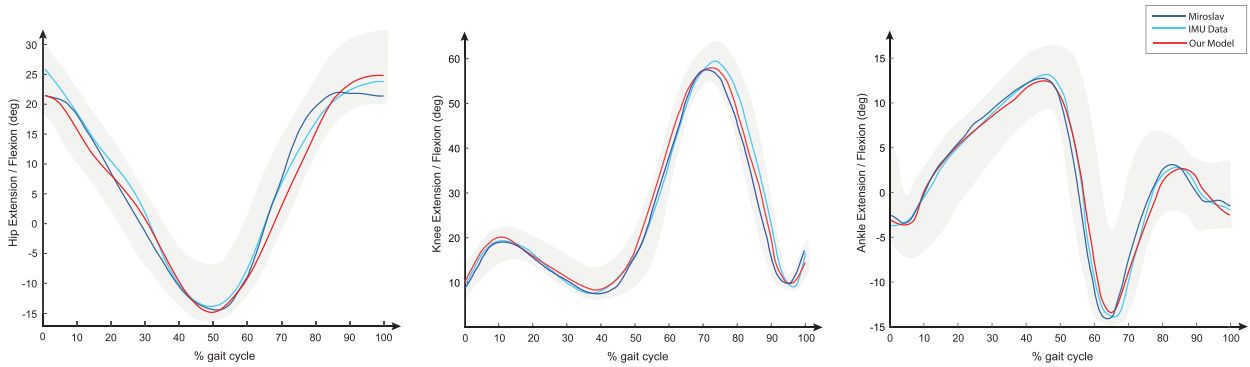


FIGURE 18. Hip flexion/extension (HFE), knee flexion/extension (KFE) and ankle flexion/extension (AFE) angular position (degrees) during a normal gait cycle.

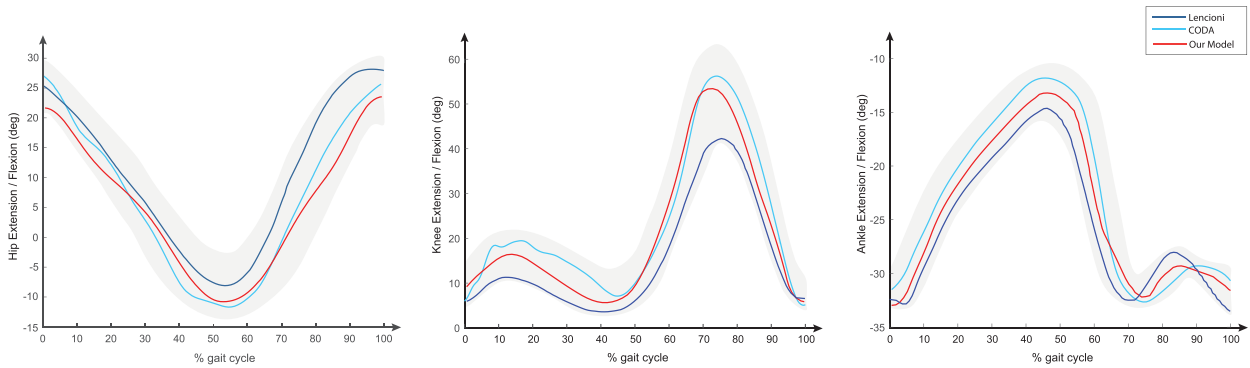


FIGURE 19. Hip flexion/extension, knee flexion/extension and ankle flexion/extension angular position (degrees) during a gait cycle for persons with multiple sclerosis.

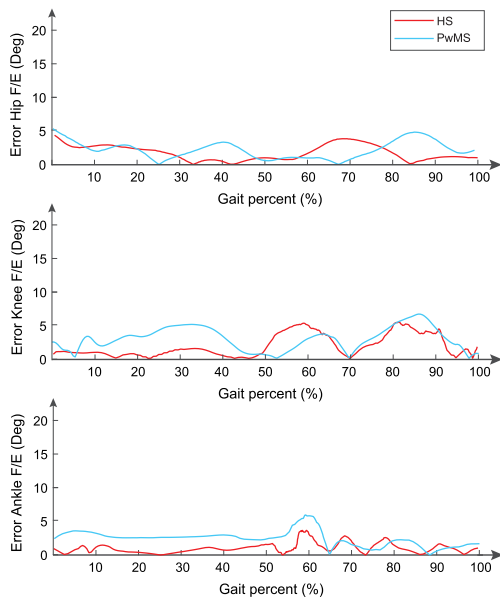


FIGURE 20. Absolute errors (degrees) obtained by our model for Hip flexion/extension, knee flexion/extension, and ankle flexion/extension, during a gait cycle for healthy subjects (HS) and persons with multiple sclerosis (PwMS).

the reference data closely, better than previously published works, suggesting a satisfactory estimation, so, the model predicts successfully for both normal and pathological gait. On the other hand, the locomotor deficits that were found

to characterize gait in PwMS are due to the changes in the activation profiles resulting in a decrease of the joint's range of motion and muscles activation delays.

IV. CONCLUSIONS

In this study, we have presented a complete musculoskeletal model using Musculoskeletal Modeling Software (MSMS) and Simulink. Musculoskeletal models are an important tool to perform biomechanical analysis and have been successfully used previously to simulate injuries, surgeries and to determine forces and torques.

Our model was validated by comparing the results with previously reported works (early models and experimental results). We compared the moment arm of muscles crossing the knee for knee flexion, maximum isometric knee flexion/extension moment, maximum isometric ankle dorsiflexion/plantarflexion moment and passive hip flexion moment.

On the other hand, the model was also validated by comparing with real data, for both normal and pathological gait. For normal gait, the value obtained by our model were compared with real data obtained from our own wireless gait capture system and with data obtained from CODA software at Physiotherapy School ONCE, as well as a previously published work.

Furthermore, the model was also validated by comparing the results obtained for people with multiple sclerosis with those obtained from previously published works

TABLE 10. Root mean square error (RMSE) and normalized mean square error (NMSE) obtained by our model and previously reported works, for both healthy and persons with multiple sclerosis.

		Hip flex/ext		Knee flex/ext		Ankle flex/ext	
		RMSE (deg)	NMSE (%)	RMSE (deg)	NMSE (%)	RMSE (deg)	NMSE (%)
Healthy subject	Miroslav	1.881	1.966	3.969	1.518	1.580	4.684
	Our model	2.222	2.743	2.793	0.752	0.961	1.736
Person with Multiple Sclerosis	Lencioni	4.831	13.178	8.50	9.224	3.774	2.455
	Our model	2.542	3.650	3.685	1.733	1.828	0.576

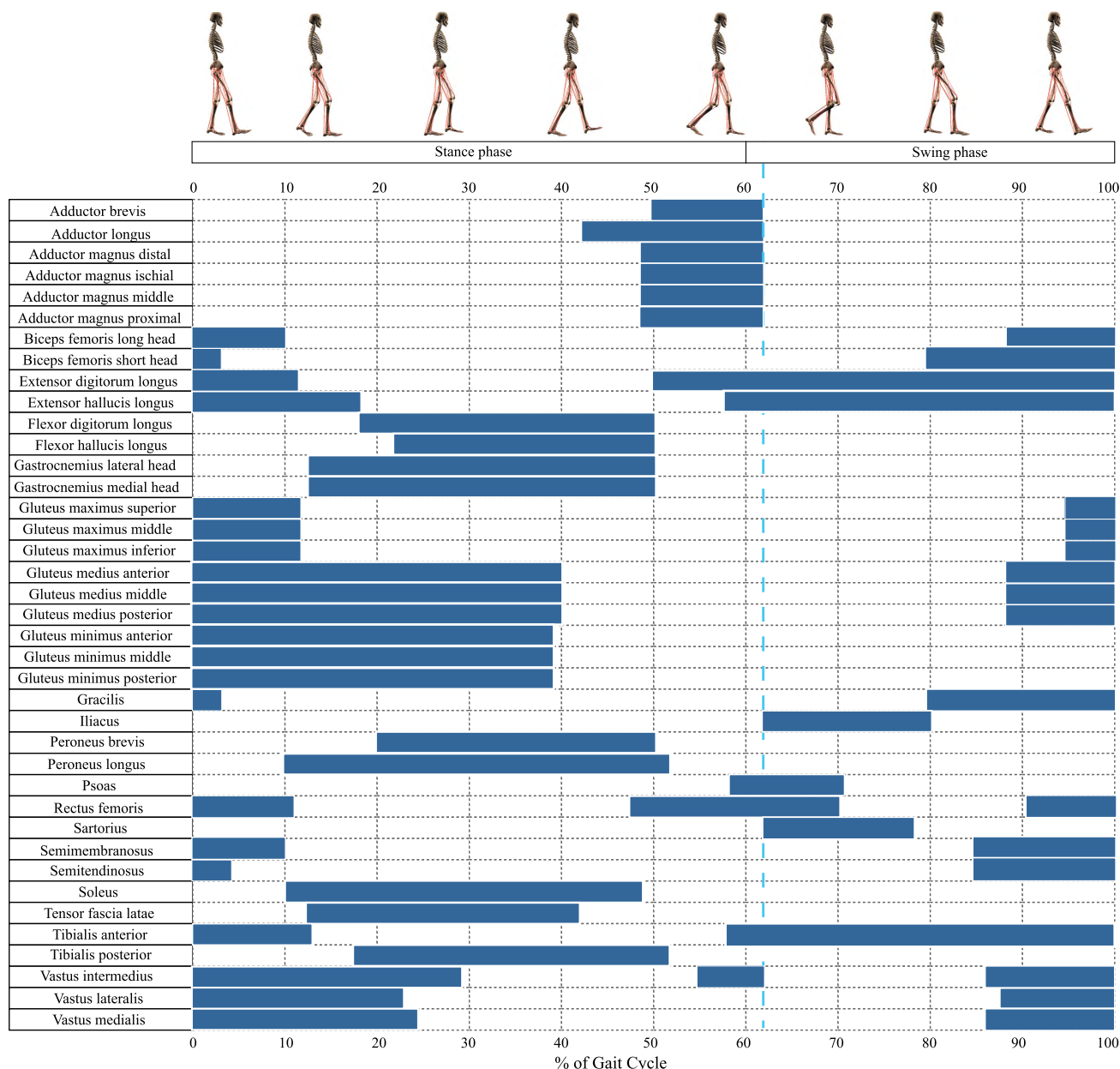


FIGURE 21. Muscle-Tendons activation signals during the gait cycle.

and from the Physiotherapy School ONCE. The goodness-of-fit of our model was assessed using the root mean square error (RMSE) and the normalized mean square error

(NMSE). For instance, for hip flexion/extension the model has an RMSE of 2.222 degrees and an NMSE of 2.743 % for normal gait respectively, whereas for pathological case

our model presents an RMSE of 2.542 degrees and an NMSE of 3.650 %. In the case of the knee flexion/extension, the RMSE was 2.793 degrees and the NMSE 0.752 % for normal gait respectively, whereas for pathological case our model presents an RMS of 3.685 degrees and an NMSE of 1.733 %. Hence, there is strong evidence that our model estimates satisfactorily, and better than previously published works, the human biomechanics for both normal and pathological subjects.

It is worth mentioning that many models are based on datasets previously reported, as in our case, however, none of the models generate identical results, this is due to the fact that, although the same morphometric values of the muscle-tendon have been used, the origin and insertion points of the muscle-tendon units, as well as the location, fiber type settings (recruitment type, apportion method, maximum recruitment excitation value), type and number of wrapping objects are not the same.

Additionally, the model can receive signals in real-time from external sources, either from sensors such as inertial measurement unit or force sensors, commercial medical devices or motion analysis systems like Codamotion. This is a very important feature for data acquisition and visualization in real-time simulations in virtual reality environments with the subject in the loop.

Furthermore, in the Simulink model, we can send activation signals to individual muscles, allowing not only estimate joint torques for actuator dimensioning and selection to design mechanism but also to test control strategies in order to implement it in rehabilitation exoskeleton robots.

Finally, with this study we have a validated model and can be used for biomechanical analysis of the human movement and robotics exoskeleton controller design, hence, in the next step we will continue performing simulations with pathological subjects, the tests will be conducted at Physiotherapy School ONCE, Madrid, in order to obtain the requirements engineering to design an exoskeleton robotics for rehabilitation.

APPENDIX A MUSCLE-TENDON ACTIVATION DURING GAIT CYCLE

The muscle-tendon activation signals, simulating the functional electrical stimulation (FES), applied into the Simulink model are shown in Fig. 21.

ACKNOWLEDGMENT

The authors would like to thanks to Physiotherapy School ONCE, Madrid and the Faculty of Medicine, Universidad Autónoma de Madrid.

REFERENCES

- [1] S. Piazza and S. Delp, "Three-dimensional dynamic simulation of total knee replacement motion during a step-up task," *J. Biomech. Eng.*, vol. 123, no. 6, pp. 599–606, 2001.
- [2] D. Cazzola, T. P. Holsgrove, E. Preatoni, H. S. Gill, and G. Trewartha, "Cervical spine injuries: A whole-body musculoskeletal model for the analysis of spinal loading," *PLoS ONE*, vol. 12, pp. 1–24, Jan. 2017.
- [3] C. Paul, M. Bellotti, S. Jezernik, and A. Curt, "Development of a human neuro-musculo-skeletal model for investigation of spinal cord injury," *Biological*, vol. 93, no. 3, pp. 153–170, 2005.
- [4] A. S. Arnold, D. J. Asakawa, and S. L. Delp, "Do the hamstrings and adductors contribute to excessive internal rotation of the hip in persons with cerebral palsy?" *Gait Posture*, no. 11, pp. 90–181, 2000.
- [5] J. A. Reinbolt, A. Seth, and S. L. Delp, "Musculoskeletal modelling in sports—Evaluation of different software tools with focus on swimming," in *Proc. 11th Conf. Int. Sports Eng. Assoc. (ISEA)*, 2016, pp. 281–287.
- [6] J. Rasmussen, L. J. Holmberg, K. Sørensen, M. Kwan, M. Andersen, and M. de Zee, "Performance optimization by musculoskeletal simulation," *Movement Sport Sci.-Sci. Motricité*, no. 75, pp. 73–83, 2012.
- [7] H.-S. Lee, J.-H. Lee, and H.-S. Kim, "Activities of ankle muscles during gait analyzed by simulation using the human musculoskeletal model," *J. Exerc. Rehabil.*, vol. 15, no. 2, pp. 229–234, 2019. [Online]. Available: <http://www.e-jer.org/journal/view.php?number=2013600670>
- [8] Y. Wang, X. Li, P. Huang, G. Li, and P. Fang, "An analysis of biomechanical characteristics of gait based on the musculoskeletal model," in *Proc. IEEE Int. Conf. Cyborg Bionic Syst. (CBS)*, Oct. 2018, pp. 151–154.
- [9] S. L. Delp, J. P. Loan, M. G. Hoy, F. E. Zajac, E. L. Topp, and J. M. Rosen, "An interactive graphics-based model of the lower extremity to study orthopaedic surgical procedures," *IEEE Trans. Biomed. Eng.*, vol. 37, no. 8, pp. 757–767, Aug. 1990.
- [10] M. K. Horsman, "The Twente lower extremity model. Consistent dynamic simulation of the human locomotor apparatus," Ph.D. dissertation, Fac. Eng. Technol., Univ. Twente, Enschede, The Netherlands, 2007.
- [11] E. M. Arnold, S. R. Ward, R. L. Lieber, and S. L. Delp, "A model of the lower limb for analysis of human movement," *Ann. Biomed. Eng.*, vol. 38, no. 2, pp. 269–279, Feb. 2010.
- [12] V. Carbone, R. Fluit, P. Pellikaan, M. M. van der Krogt, D. Janssen, M. Damsgaard, L. Vigneron, T. Feilkas, H. F. J. M. Koopman, and N. Verdonschot, "TLEM 2.0—A comprehensive musculoskeletal geometry dataset for subject-specific modeling of lower extremity," *J. Biomech.*, vol. 48, no. 5, pp. 734–741, 2015.
- [13] A. Rajagopal, C. L. Dembia, M. S. DeMers, D. D. Delp, J. L. Hicks, and S. L. Delp, "Full-body musculoskeletal model for muscle-driven simulation of human gait," *IEEE Trans. Biomed. Eng.*, vol. 63, no. 10, pp. 2068–2079, Oct. 2016.
- [14] G. Handsfield, C. H. Meyer, J. Hart, M. Abel, and S. S. Blemker, "Relationships of 35 lower limb muscles to height and body mass quantified using MRI," *J. Biomech.*, vol. 47, no. 3, pp. 631–638, 2014.
- [15] S. R. Ward, C. M. Eng, L. H. Smallwood, and R. L. Lieber, "Are current measurements of lower extremity muscle architecture accurate?" *Clin. Orthopaedics Rel. Res.*, vol. 467, no. 4, pp. 1074–1082, 2009.
- [16] A. K. M. Lai, A. S. Arnold, and J. M. Wakeling, "Why are antagonist muscles co-activated in my simulation? A musculoskeletal model for analysing human locomotor tasks," *Ann. Biomed. Eng.*, vol. 45, no. 12, pp. 2762–2774, 2017.
- [17] *International Ethical Guidelines for Biomedical Research Involving Human Subjects*, CIOMS, Geneva, Switzerland, 2002.
- [18] M. A. Destarac, C. E. G. Cena, R. J. S. Pazmiño, M. J. R. Urbina, J. L. López, and R. E. Gómez, "Modeling and simulation of upper brachial plexus injury," *IEEE Syst. J.*, vol. 10, no. 3, pp. 912–921, Sep. 2016.
- [19] L. Modenese, A. T. M. Phillips, and A. M. J. Bull, "An open source lower limb model: Hip joint validation," *J. Biomech.*, vol. 44, no. 12, pp. 2185–2193, 2011.
- [20] R. Chauhan and J. Vyas, "Lower limb musculoskeletal modeling for standing and sitting event by using musculoskeletal modeling software," *GIT-J. Eng. Technol.*, vol. 6, no. 2, pp. 201–206, 2013.
- [21] M. Millard, T. Uchida, A. Seth, and S. Delp, "Flexing computational muscle: Modeling and simulation of musculotendon dynamics," *ASME, J. Biomech. Eng.*, vol. 135, no. 2, p. 021005, Feb. 2013.
- [22] Q. Zhang, X. Wang, M. Tian, X. Shen, and Q. Wu, "Modeling of novel compound tendon-sheath artificial muscle inspired by hill muscle model," *IEEE Trans. Ind. Electron.*, vol. 65, no. 8, pp. 6372–6381, Aug. 2018.
- [23] Z. Shao, Q. Wu, B. Chen, and H. Wu, "Force and deformation transmission characteristics of a compliant tendon-sheath actuation system based on Hill-type muscle model," *Proc. Inst. Mech. Eng. H, J. Eng. Med.*, to be published. doi: [10.1177/0954411919847052](https://doi.org/10.1177/0954411919847052).
- [24] R. Kelc, J. Naranda, K. Matevz, and M. Vogrin, *The Physiology of Sports Injuries and Repair Processes*. London, U.K.: IntechOpen, 2013, pp. 43–86. doi: [10.5772/54234](https://doi.org/10.5772/54234).

- [25] L. Blankevoort, J. Kuiper, R. Huiskes, and H. Grootenboer, "Articular contact in a three-dimensional model of the knee," *J. Biomech. Eng.*, vol. 24, no. 11, pp. 1019–1031, 1991.
- [26] K. Barfod, "Achilles tendon rupture; assessment of nonoperative treatment," *Danish Med. J.*, vol. 61, p. B4837, Jan. 2014.
- [27] H. Katherine, T. Guess, L. Maletsky, and K. Dodd, "Computational knee ligament modeling using experimentally determined zero-load lengths," *J. Biomech. Eng.*, vol. 6, pp. 33–41, Apr. 2012.
- [28] D. Stanev, K. Moustakas, J. Gliatis, and C. Koutsojannis, "ACL reconstruction decision support personalized simulation of the lachman test and custom activities," *Methods Inf. Med.*, vol. 55, no. 1, pp. 98–105, 2016.
- [29] A. Kapandji, *Fisiología Articular*, vol. 2, 6th ed. Paris, France: Editorial Panamericana, 2010.
- [30] K. Moromizato, R. Kimura, H. Fukase, K. Yamaguchi, and H. Ishida, "Whole-body patterns of the range of joint motion in young adults: Masculine type and feminine type," *J. Physiol. Anthropol.*, vol. 35, pp. 1–12, Oct. 2016.
- [31] M. A. Destarac, C. E. G. Cena, J. Garcia, R. Espinoza, and R. J. Saltaren, "ORTE: Robot for upper limb rehabilitation. Biomechanical analysis of human movements," *IEEE Latin Amer. Trans.*, vol. 16, no. 6, pp. 1638–1643, Jun. 2018.
- [32] J. W. L. Buford, Jr. F. M. Ivey, Jr., J. D. Malone, R. M. Patterson, G. L. Peare, D. K. Nguyen, and A. A. Stewart, "Muscle balance at the knee—moment arms for the normal knee and the ACL-minus knee," *IEEE Trans. Rehabil. Eng.*, vol. 5, no. 4, pp. 367–379, Dec. 1997.
- [33] C. W. Spoor and J. L. van Leeuwen, "Knee muscle moment arms from MRI and from tendon travel," *J. Biomech.*, vol. 25, pp. 201–206, 1992.
- [34] D. E. Anderson, M. L. Madigan, and M. A. Nussbaum, "Maximum voluntary joint torque as a function of joint angle and angular velocity: Model development and application to the lower limb," *J. Biomech.*, vol. 40, no. 14, pp. 3105–3113, 2007.
- [35] R. Riener and T. Edrich, "Identification of passive elastic joint moments in the lower extremities," *J. Biomech.*, vol. 32, no. 5, pp. 539–544, 1999.
- [36] M. Murray, G. M. Gardner, L. A. Mollinger, and S. B. Sepic, "Strength of isometric and isokinetic contractions: Knee muscles of men aged 20 to 86," *Phys. Therapy*, vol. 60, no. 4, pp. 412–419, 1980.
- [37] T. M. van Eijden, W. Weijs, E. Kouwenhoven, and J. Verburg, "Forces acting on the patella during maximal voluntary contraction of the quadriceps femoris muscle at different knee flexion/extension angles," *Acta Anat (Basel)*, vol. 129, no. 4, pp. 310–314, 1987.
- [38] E. Marsh, D. Sale, A. McComas, and J. Quinlan, "Influence of joint position on ankle plantarflexion in humans," *J. Appl. Physiol.*, vol. 51, no. 6, pp. 160–167, 1981.
- [39] D. Sale, J. Quinlan, E. Marsh, A. McComas, and A. Belanger, "Influence of joint position on ankle plantarflexion in humans," *J. Appl. Physiol.*, vol. 52, no. 6, pp. 1636–1642, 1982.
- [40] J. Miroslav, C. Lee, S. Zdenek, K. Jitka, and G. Anna, "Kinematic analysis of gait in patients with juvenile hallux valgus deformity," *J. Biomech. Sci. Eng.*, vol. 3, no. 3, pp. 390–398, 2008.
- [41] T. Lencioni, J. Jonsdottir, D. Cattaneo, A. Crippa, E. Gervasoni, M. Rovaris, E. Bizzi, and M. Ferrarin, "Are modular activations altered in lower limb muscles of persons with multiple sclerosis during walking? Evidence from muscle synergies and biomechanical analysis," *Frontiers Hum. Neurosci.*, vol. 10, pp. 1–14, Dec. 2016.



MANUEL CARDONA (M'09–SM'15) received the B.S. degree in electrical engineering from the Universidad de Sonsonate (USO), El Salvador, in 2004, and the M.Sc. degree in automation and robotics from the Universidad Politécnica de Madrid, Madrid, Spain, in 2008, where he is currently pursuing the Ph.D. degree in automation and robotics.

From 2007 to 2008, and in 2011, he was a Research Assistant with the Robotics and Intelligence Machines Research Group, Universidad Politécnica de Madrid. He has a Postgraduate Certificate in Scientific Research and a Postgraduate Degree and Innovation Management. Since 2014, he has been a Professor and the Director of the Robotics and Intelligence Machines Research Group and the Computer Vision Research Group, School of Engineering, Universidad Don Bosco (UDB), El Salvador. His research interests include rehabilitation robotics, biomechanics, kinematic and dynamic of serial and parallel robots, embedded systems, vision and artificial intelligence, and applications of robotics systems.

Mr. Cardona belongs to the Robotics and Automation Society (RAS), the Aerospace and Electronic Systems Society (AESS), and the Education Society (EdSOC). He is also an IEEE RAS and AESS Student Branch Chapter Advisor at the Universidad Don Bosco and the EdSOC Chair at the IEEE El Salvador Section.



CECILIA E. GARCÍA CENA received the B.S. degree in electromechanics engineering from La Pampa National University, Santa Rosa, Argentina, in 1997, and the Ph.D. degree in control system (curriculum in robotics and nonlinear system control) from San Juan National University, San Juan, Argentina, in 2001. In 2001, she was a Visiting Scholar with the Robotics Section, Universidad Politécnica de Madrid (UPM-CSIC), Madrid, Spain. In 2004, she was a Visiting Professor with the Robotics Laboratory, Universidad Carlos III de Madrid, Madrid. She is currently an Assistant Professor with the Department of Electronics, Automation and Computer Science, UPM-CSIC, and a member of the Centre of Automation and Robotics, UPM-CSIC. Her research interests include telerobotics, assistant robots, and control of multiagent systems. She holds three patents and is the author of more than 20 articles.

...